Ultrasonics 131 (2023) 106933

Contents lists available at ScienceDirect

Ultrasonics

journal homepage: www.elsevier.com/locate/ultras

An improved analytic model for designing the polymer-composite stepped-plate transducer using the modified Mindlin plate theory

Beomseok Oh [a], Chayeong Kim [a], Dongwoo Lee [a], Junsuk Rho [a,b,c,*], Wonkyu Moon [a,*]

[a] Department of Mechanical Engineering, Pohang University of Science and Technology (POSTECH), Pohang 37673, Republic of Korea
[b] Department of Chemical Engineering, Pohang University of Science and Technology (POSTECH), Pohang 37673, Republic of Korea
[c] POSCO-POSTECH-RIST Convergence Research Center for Flat Optics and Metaphotonics, Pohang 37673, Republic of Korea

ARTICLE INFO

Keywords:
Stepped-plate transducer
High-power ultrasonic transducer
Piezoelectric transducer
Plate theory

ABSTRACT

A stepped-plate transducer (SPT) uses an extensive radiating plate to produce highly-directional ultrasound beams. In this paper, we present an improved analytical model for designing the polymer-composite stepped-plate transducer (PCSPT). The polymer-composite features the lightweight and flexible properties, and there can be little change in the resonant frequency and mode shape when the steps are attached. With the outstanding merit, it is feasible to construct SPTs with polymer-composite steps without taking the steps into consideration. The modified Mindlin plate theory (MMPT) is applied to improve the accuracy in the equivalent circuit model (ECM) that is used to predict the high-frequency vibratory responses. Our analytical model can be used to design well-tuned SPTs to achieve the desired dynamic responses such as resonant frequencies, mode shape and bandwidth for various high-power ultrasonic applications. We use several numerical design examples to illustrate that the design of the transducer can be accomplished without analyzing the sophisticated stepped-plate's behavior. We also perform a series of experiments to verify that the PCSPT is capable of functioning as a high-power ultrasonic transducer.

1. Introduction

The stepped-plate transducer (SPT) [1] is a useful radiator for in-air high-power ultrasonic applications, e.g., ultrasonic agglomeration [2], acoustic levitation [3], distance ranging [4,5], defoaming [6], dehydration [7], and harmonic radiation force generator [8]. It has a relatively simple structure that uses only one actuating part, so it can be manufactured at lower cost than other generators of airborne ultrasound [9]. SPT can radiate intensive sound beams in air at a relatively high power-efficiency, but design of a decent SPT for a given target frequency can be a difficult task. To maximize the strength of radiated sound beams, the SPT for mono-frequency sound beams should be so designed that the chosen operating frequency of the stepped-plate is well matched with the resonance frequencies of the Langevin transducer that uses a mechanical horn [10]. However, to meet this requirement entails the difficulty of designing a stepped circular plate that has a desired vibration mode shape when excited in the axial direction of the circular plate [10,11]. Consequently, development of a well-designed SPT with a given operating frequency and a desired strength of emitted sound beams, is an important research goal [12].

The conventional SPT can be modified for use as a wide-band ultrasound beam radiator [9–11]. If the ultrasonic beam radiates at two frequencies, their nonlinear interaction can be exploited to generate a difference frequency wave [9]; this phenomenon is, called a parametric array (PA) [13]. The SPT can be used as a kind of PA loudspeaker [10] if appropriate changes are adopted in the design processes so that its multiple resonances would closely placed in the frequency domain; this change widens the bandwidth by exploiting the multi-resonant phenomenon that is caused by closely-spaced resonant frequencies [10]. The target application requires wide-band ultrasounds, which can be generated by a different kind of tuning process to match the resonance frequencies of the stepped-plate and the actuating part. During the design process, the most difficult part is to identify the geometry of a stepped-plate to resonate at a target frequency with a desired mode shape and height of steps at desired locations on a circular plate. One option is to use a stepped-plate in which the step parts have smaller total volume than the flat part of the plate, but this method requires a considerably thick plate, which causes low vibration amplitude and parasitic vibration mode excitation [10].

Recently, it is reported that the steps composed of the polymer-type composite material that has sufficiently small density and Young's modulus might avoid considerable changes to the resonance frequencies

* Corresponding authors.
E-mail addresses: bs.oh@postech.ac.kr (B. Oh), kcycj@postech.ac.kr (C. Kim), dwlee93@postech.ac.kr (D. Lee), jsrho@postech.ac.kr (J. Rho), wkmoon@postech.ac.kr (W. Moon).

https://doi.org/10.1016/j.ultras.2023.106933
Received 15 December 2022; Received in revised form 11 January 2023; Accepted 18 January 2023
Available online 24 January 2023
0041-624X/© 2023 Elsevier B.V. All rights reserved.

and corresponding vibration mode shapes [11]. A polymer-composite step can be molded easily on the flat circular plate, and a polymer-composite stepped-plate transducer (PCSPT) made by such technique might almost preserve the desired resonance frequencies and mode shapes [11]. This result implies that the flat plate model can be substitute for that of the stepped-plate and might reduce the burden in the design process of the stepped-plate PA loudspeaker because a precise theoretical model such as the ECM has been already developed for the flat plate transducer (FPT) [14]. Consequently, the analytical model for a flat plate would be useful in design analyses to predict the dynamic behaviors of SPTs, if the polymer composite steps are fabricated on the flat circular plate to make a desired stepped-plate. Although the polymer-composite stepped-plate technology was introduced for PA loudspeaker applications [11], it can be used for a conventional SPT that emits mono-frequency ultrasonic beams, so the FPT model can be also applied to design processes for the conventional SPT. When applied to conventional SPT, the existing FPT model [14] does not calculate resonance frequencies of the high vibration modes accurately enough to predict the dynamic behaviors of SPT. This inaccuracy impedes design of a well-tuned SPT to achieve the required dynamic responses. This failure indicates the need to develop a design model to that can precisely predict the vibratory behaviors of the whole SPT, in addition to its resonance frequencies and the corresponding vibration modes of a flat plate.

In this paper, the modified Mindlin plate theory (MMPT) [15] is used to improve the accuracy in the ECM that is used to predict the vibration responses of SPT that is operated at high bending-mode frequency. This model is much more accurate than the previous FPT model based on the classical plate theory [14] in predicting resonance frequencies and their corresponding mode shapes. The benefit of the new model is evaluated by applying to the design processes for a conventional SPT and a stepped-plate PA loudspeaker.

2. Polymer composite stepped-plate transducer (PCSPT)

In general, the resonance frequency of the radiation plate is changed significantly when the steps are attached, because they are manufactured of the same metal as the plate [10]. Especially, unpredictable mode shapes occur if the plate is thinner than the height of the steps [11]. Because of these changes, appropriate phase compensation is impossible, so the development of directional sound waves is restricted. Therefore, the plate's thickness must be comparable to the height of the steps [10]. The acoustic radiation efficiency can be increased by thinning the plate [10], but this approach is not possible in conventional SPTs. Heat generation can also degrade the vibration amplitude of the transducer. The driving part of the SPT is a Langevin transducer, which is a piezoelectric sandwich transducer. Langevin transducers mainly use piezoelectric ceramics that have high electromechanical coupling coefficient and low dielectric loss to generate high-amplitude vibration [16]. These piezoceramics have a very small dielectric loss (about 0.2~0.3%). However, in high-voltage operation conditions, dielectric loss increases significantly due to the strong electric field and consequent high vibration stress [17–20], which leads to heat generation and resonant frequency transition [21,22]. Therefore, the device must be equipped with a heat sink or other cooling device [11,23].

These design constraints can be overcome by using a SPT in which the steps are composed of polymer-composite rather than the same metal as the plate. If a polymer-type composite material has light and flexible mechanical properties, then the polymer-composite steps can have negligible effects on the resonance frequency and the mode shape [11]. In addition, mechanical damping by the polymer-composite steps effectively suppresses the heat generation of the piezoelectric ceramics, and thus avoids the resonant frequency transition and vibration amplitude degradation [11]. This result shows that the required bending mode and target frequency can be obtained by considering only the flat plate, so the process is thus much simpler than design of the general SPT.

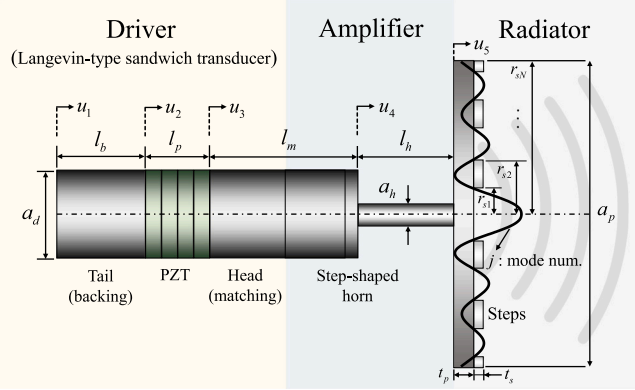

Fig. 1. Schematic diagram of the polymer-composite stepped-plate transducer (PCSPT).

3. Theoretical analysis for transducer design

3.1. Transducer components

The proposed transducer (refer to Fig. 1 and Table A.1) consists of three parts: driver, amplifier, and radiating plate. Aluminum and steel are mainly used for matching and backing. For piezoelectric ceramics, lead zirconate titanate (PZT) is widely used for high-power applications because of its high Q-factor and piezoelectric constants [24,25]. The vibration displacement of the Langevin transducer is amplified by a horn and then transmitted to the radiating plate. We use a step-type horn, which is a standard structure for conventional piezoelectric ultrasonic transducers.

3.2. High-frequency vibratory radiating plate with moderate thickness: A theoretical model for the radiating plate

In this section, we discuss the plate theory to analyze the dynamic behavior of the radiating plate. The Kirchhoff plate theory, also called classical plate theory (CPT), which is the fundamental theory of plates and has been widely used to analyze their mechanical behavior [26]. CPT assumes a thin plate and ignores transverse shear deformation and rotary inertia. However, at higher-order vibration mode or when plate thickness is increased, these effects also increase; CPT would then produce a significant error [27–31]. Usually, the radiation plate of the stepped-plate transducer undergoes high-frequency flexural vibration [1,8–11,32]; therefore, CPT may not be applicable. To accurately predict the behavior of the radiation plate in a PCSPT, transverse shear deformation and rotary inertia effects must be included. Mindlin–Reissner plate theory [31,33] is a well-known conventional theory that considers the shear deformation and the rotary inertia effects; it is generally recognized as being suitable for moderately thick, high-frequency vibration plates. Various studies have been published on the plate theory subsequent to the work of Mindlin and Reissner; Liew et al. performed a literature review on plate theories [34].

3.2.1. Modified Mindlin plate theory (MMPT)

In this work, we model the radiating plate by using the MMPT [15], which divides the displacement into pure bending deflection, shear deflection, bending rotations, and in-plane shear angles [15,35,36]. Three partial differential equations of motion in MMPT can be reduced to a single equation with that has only the bending displacement as a fundamental variable; the remaining components, namely the angles of rotation and shear deflection, can be expressed as potential functions with respect to the bending displacement. These simplifications reduce the computational cost of solving plate problems, and thereby increases the efficiency of analysis. In a PCSPT, the mechanical horn acts as a vibration amplifier that excites the center of the plate; therefore,

we can consider a center-excited axisymmetric free-edge plate [11]. The reduced equation for flexural vibrations in the polar coordinates is [15,36]

$$\Delta_r\Delta_r W_b + \omega^2 \frac{J}{D}\left(1+\frac{\overline{m}D}{JS}\right)\Delta_r W_b + \omega^2\frac{\overline{m}}{D}\left(\frac{\omega^2 J}{S}-1\right)W_b = 0, \tag{1}$$

where $\Delta_r(\cdot) = \partial^2(\cdot)/\partial r^2 + (1/r)\partial(\cdot)/\partial r$ is the Laplacian operator, $J = \rho(h^3/12)$ is the mass moment of inertia of the cross section with unit breadth, where h indicates the plate thickness, $\overline{m} = \rho h$ is the plate mass per unit area, $D = Eh^3/[12(1-\nu^2)]$ is the flexural rigidity, and $S = \kappa G h$ is the shear stiffness with the shear correction coefficient $\kappa = 5/(6-\nu)$ [37]. By introducing parameters λ and χ, Eq. (1) can be expressed as

$$(\Delta_r + \lambda^2)(\Delta_r - \chi^2)W_b = 0. \tag{2}$$

Eq. (1) and Eq. (2) are identical, so

$$\lambda^2 = \frac{1}{2}\left[\left\{\omega^4\left(\frac{J}{D}\right)^2\left(1+\frac{\overline{m}D}{JS}\right)^2 + 4\omega^2\frac{\overline{m}}{D}\left(1-\omega^2\frac{J}{S}\right)\right\}^{\frac{1}{2}} + \omega^2\frac{J}{D}\left(1+\frac{\overline{m}D}{JS}\right)\right],$$
$$\chi^2 = \frac{1}{2}\left[\left\{\omega^4\left(\frac{J}{D}\right)^2\left(1+\frac{\overline{m}D}{JS}\right)^2 + 4\omega^2\frac{\overline{m}}{D}\left(1-\omega^2\frac{J}{S}\right)\right\}^{\frac{1}{2}} - \omega^2\frac{J}{D}\left(1+\frac{\overline{m}D}{JS}\right)\right]. \tag{3}$$

By substituting $\lambda = \xi/r$ and $\chi = \eta/r$ in Eq. (2), Bessel's differential equation and modified Bessel's differential equation can be expressed, respectively, as

$$\frac{d^2W_b}{d\xi^2} + \frac{1}{\xi}\frac{dW_b}{d\xi} + W_b = 0, \quad \frac{d^2W_b}{d\eta^2} + \frac{1}{\eta}\frac{dW_b}{d\eta} - W_b = 0. \tag{4}$$

From Eq. (4), the general solution can be expressed as a linear combination of the Bessel function of the first kind and the modified Bessel function of the first kind,

$$W_b = C_1 J_0(\xi) + C_2 I_0(\eta). \tag{5}$$

The total bending deflection $W = W_b + W_s$ can be expressed using Eq. (5) and the Fourier transformation of the shear deflection $w_s = -\Delta w_b(D/S) + (J/S)(\partial^2 w_b/\partial t^2)$ [15] as

$$W = \left(1-\omega^2\frac{J}{S}\right)\left[C_1 J_0(\xi) + C_2 I_0(\eta)\right] - C_1\frac{D}{S}\lambda^2\left[J_0''(\xi) + J_0'(\xi)/\xi\right] - C_2\frac{D}{S}\chi^2\left[I_0''(\eta) + I_0'(\eta)/\eta\right]. \tag{6}$$

The bending moment and effective shear force can be expressed as

$$\begin{aligned} M_r &= -D\left(\frac{d^2W_b}{dr^2} + \frac{\nu}{r}\frac{dW_b}{dr}\right) \\ &= -C_1 D\lambda^2\left(J_0''(\xi) + \frac{\nu}{\xi}J_0'(\xi)\right) - C_2 D\chi^2\left(I_0''(\eta) + \frac{\nu}{\eta}I_0'(\eta)\right), \\ \overline{Q}_r &= -D\left(\frac{d^3W_b}{dr^3} + \frac{1}{r}\frac{d^2W_b}{dr^2} - \frac{1}{r^2}\frac{dW_b}{dr}\right) - \omega^2 J\frac{dW_b}{dr} \\ &= -C_1 D\lambda^3\left(J_0'''(\xi) + \frac{J_0''(\xi)}{\xi} - \frac{J_0'(\xi)}{\xi^2}\right) \\ &\quad - C_2 D\chi^3\left(I_0'''(\eta) + \frac{I_0''(\eta)}{\eta} - \frac{I_0'(\eta)}{\eta^2}\right) \\ &\quad - \omega^2 J\left[C_1\lambda J_0'(\xi) + C_2\chi I_0'(\eta)\right]. \end{aligned} \tag{7}$$

3.2.2. Modal analysis: Free-edge circular plate

The radiating plate undergoes flexural vibration by center excitation; therefore, the free-edge boundary conditions must be considered. Applying the boundary conditions ($M_r|_{r=R} = 0$, $\overline{Q}_r|_{r=R} = 0$) in Eq. (7) yields

$$\begin{aligned} &C_1\left(\lambda^2 J_0''(\lambda R) + \frac{\nu\lambda}{R}J_0'(\lambda R)\right) + C_2\left(\chi^2 I_0''(\chi R) + \frac{\nu\chi}{R}I_0'(\chi R)\right) = 0, \\ &C_1\left[D\left(\lambda^3 J_0'''(\lambda R) + \frac{\lambda^2}{R}J_0''(\lambda R) - \frac{\lambda}{R^2}J_0'(\lambda R)\right) + \omega^2 J\lambda J_0'(\lambda R)\right] + \\ &C_2\left[D\left(\chi^3 I_0'''(\chi R) + \frac{\chi^2}{R}I_0''(\chi R) - \frac{\chi}{R^2}I_0'(\chi R)\right) + \omega^2 J\chi I_0'(\chi R)\right] = 0. \end{aligned} \tag{8}$$

Eq. (8) forms an eigenvalue problem, which can be expressed in matrix form

$$\begin{aligned} &\begin{bmatrix} K_{11} & K_{12} \\ K_{21} & K_{22}\end{bmatrix}\begin{Bmatrix} C_1 \\ C_2\end{Bmatrix} = \{\mathbf{0}\}, \\ &K_{11} = \lambda^2 J_0''(\lambda R) + \frac{\nu\lambda}{R}J_0'(\lambda R), \quad K_{12} = \chi^2 I_0''(\chi R) + \frac{\nu\chi}{R}I_0'(\chi R), \\ &K_{21} = D\left(\lambda^3 J_0'''(\lambda R) + \frac{\lambda^2}{R}J_0''(\lambda R) - \frac{\lambda}{R^2}J_0'(\lambda R)\right) + \omega^2 J\lambda J_0'(\lambda R), \\ &K_{22} = D\left(\chi^3 I_0'''(\chi R) + \frac{\chi^2}{R}I_0''(\chi R) - \frac{\chi}{R^2}I_0'(\chi R)\right) + \omega^2 J\chi I_0'(\chi R), \end{aligned} \tag{9}$$

where C_1 and C_2 are the constants of the eigenvector that will be fixed by the boundary conditions. Solving this problem yields the natural frequencies and mode shapes.

3.2.3. Harmonic analysis: Mechanical impedance of the plate

In this section, we derive the mechanical impedance of the plate serving as the mechanical load. This impedance function will be applied to the electro-mechanical equivalent circuit model. The total deflection (Eq. (6)) can be expressed as a mode function W_i that has amplitude parameter A_i and mode shape parameter B_i, as

$$\begin{aligned} W_i = A_i\Bigg[&\left\{\left(1-\omega_i^2\frac{J}{S}\right)J_0(\lambda_i r) - \lambda_i^2\frac{D}{S}\left(J_0''(\lambda_i r) + \frac{J_0'(\lambda_i r)}{\lambda_i r}\right)\right\} + \\ &B_i\left\{\left(1-\omega_i^2\frac{J}{S}\right)I_0(\chi_i r) - \chi_i^2\frac{D}{S}\left(I_0''(\chi_i r) + \frac{I_0'(\chi_i r)}{\chi_i r}\right)\right\}\Bigg], \end{aligned} \tag{10}$$

where i indicates the mode number. B_i can be written as

$$\begin{aligned} B_i &= -\left(\frac{K_{11}}{K_{12}}\right)_i = -\left(\frac{K_{21}}{K_{22}}\right)_i = -\frac{\lambda_i^2}{\chi_i^2}\left(\frac{J_0''(\lambda_i R) + [\nu/\lambda_i R]\,J_0'(\lambda_i R)}{I_0''(\chi_i R) + [\nu/\chi_i R]\,I_0'(\chi_i R)}\right) \\ &= -\frac{\lambda_i^3}{\chi_i^3}\left(\frac{D\left[J_0'''(\lambda_i R) + J_0''(\lambda_i R)/\lambda_i R - J_0'(\lambda_i R)/(\lambda_i R)^2\right] - \omega_i^2 J\lambda_i J_0'(\lambda_i R)}{D\left[I_0'''(\chi_i R) + I_0''(\chi_i R)/\chi_i R - I_0'(\chi_i R)/(\chi_i R)^2\right] - \omega_i^2 J\chi_i I_0'(\chi_i R)}\right), \end{aligned} \tag{11}$$

where C_i and K_{ij} (where i, $j = 1$ and 2) are given in Eq. (9), and A_i can be expressed as [38]

$$\iint_S \rho h W_i^2\, dS = m,$$
$$A_i^2 = \frac{R^2}{2}\left(\int_0^R r[\{(1-\omega_i^2 J/S)J_0(\lambda_i r) - D\lambda_i^2/S(J_0''(\lambda_i r) + J_0'(\lambda_i r)/\lambda_i r)\} + B_i\{(1-\omega_i^2 J/S)I_0(\chi_i r) - D\chi_i^2/S(I_0''(\chi_i r) + I_0'(\chi_i r)/\chi_i r)\}]^2 dr\right)^{-1}. \tag{12}$$

We integrate Eq. (12) to obtain the explicit form by using Mathematica program of Wolfram Research, and the resulting A_i^{-2} can be expressed as

$$\begin{aligned} A_i^{-2} = \frac{1}{S}\Bigg[&\vartheta_i^2\left\{J_0^2(\lambda_i R) + J_1^2(\lambda_i R)\right\} + B_i^2\varphi_i^2\left\{I_0^2(\chi_i R) - I_1^2(\chi_i R)\right\} \\ &- 4\frac{B_i}{R}\frac{\chi_i\vartheta_i\varphi_i}{\lambda_i^2+\chi_i^2}\left\{J_0(\lambda_i R)I_1(\chi_i R) + J_1(\lambda_i R)I_0(\chi_i R)\right\}\Bigg], \end{aligned} \tag{13}$$

where, σ_i, ϑ_i and φ_i are three introduced expressions

$$\sigma_i = \omega_i^2\frac{J}{S} - 1, \quad \vartheta_i = D\lambda_i^2 - \sigma_i S, \quad \varphi_i = D\chi_i^2 + \sigma_i S. \tag{14}$$

Next we use the modal superposition method to analyze the forced vibration response or frequency response function (FRF), where the

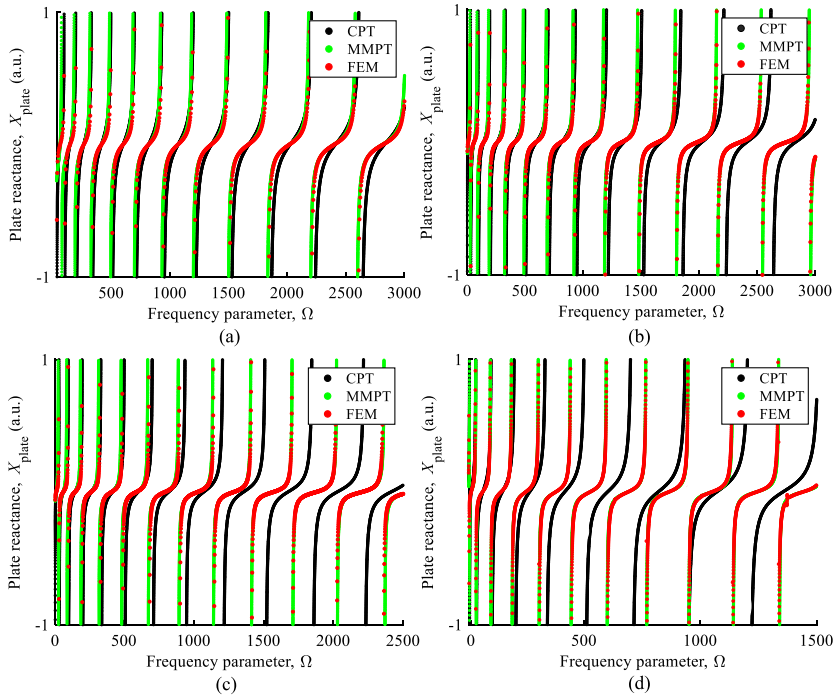

Fig. 2. Mechanical impedance of plates according to h/R and the frequency parameter Ω. X_{plate} indicates the reactance of the plates, which is the imaginary part of the impedance. (a) $h/R = 0.005$, (b) $h/R = 0.01$, (c) $h/R = 0.02$, and (d) $h/R = 0.05$.

plate's response is described by linear combinations of the vibration modes $W_i(r)$ and the natural frequencies ω_i [38–42],

$$H(r,\omega) = F\sum_{i=0}^{\infty}\frac{W_i(r_0)W_i(r)}{\rho\pi R^2 h(\omega_i^2-\omega^2+2j\zeta_i\omega_i\omega)}, \tag{15}$$

where H is a function of the driving point r_0 and the response point r, and ζ_i indicates damping ratio. For the radiating plate in PCSPT, the horn excites the center point, and the desired response point is the same. Thus, Eq. (15) can be rewritten as

$$\overline{H} = F\sum_{i=0}^{\infty}\frac{\left(W_i|_{r=0}\right)^2}{\rho\pi R^2 h(\omega_i^2-\omega^2+2j\zeta_i\omega_i\omega)}. \tag{16}$$

Finally, we obtain the driving point mechanical impedance of the plate as

$$Z_{\text{plate}} = \frac{F}{j\omega\overline{H}}. \tag{17}$$

In Fig. 2, we show several mechanical impedance (lossless, pure imaginary reactance) curves of the aluminum plates according to h/R and the frequency parameter, which is defined by $\Omega = \omega R^2\sqrt{\rho h/D}$. If the reactance of a plate goes to zero, the mechanical resonance states have been reached; conversely, if the reactance reaches infinity, anti-resonant states have been reached. Results obtained using FEM, CPT, and MMPT all have good accuracy for $h/R = 0.005$ (thin plate), but as h/R increases, the accuracy of CPT decreases, whereas the results of MMPT remain the same as those of FEM. As discussed, SPTs operate at ultrasonic frequency, so use of MMPT is appropriate regardless of plate thickness as well as the operating frequency.

3.3. Equivalent circuit model

In this section, we describe the ECM for combining the radiating plate and Langevin-type piezoelectric transducer. An ECM is an effective method for investigating the frequency response of an ultrasonic transducer [12,43–47]. The components of the transducer (Fig. 1) can be expressed using an ECM. Several studies have been conducted to establish ECM for flat plate radiators [14,48]. Transducers with radiating plates that behave in high-order bending modes cannot fully exploit of the results from [48], because it considered only the lowest bending mode of the plate. An ECM that includes radiating plates with high-order modes [14] cannot be implemented when the ratio h/R is not sufficiently small or at high-frequency operation because the mechanical behavior of the plates was investigated using CPT. In the following section, we use design examples to demonstrate the high accuracy of our newly-developed ECM across a wide range of plate dimensions and operating frequencies. The overall behavior of the transducers can be understood by combining the driving part and the mechanical impedance of the plate derived from the MMPT. The ECM of the transducer (Fig. 3) does not include the steps because the polymer-composite steps have little effect on the resonance frequency and mode shape of the plate; therefore, a flat plate without steps can be considered [11]. The expressions for the series and parallel impedance in Fig. 3 are

$$\begin{aligned}
&Z_{b1} = Z_{b2} = jZ_{b0}\tan(k_b l_b/2), \quad Z_{p1} = Z_{p2} = jZ_{p0}\tan(k_p l_p/2),\\
&Z_{m1} = Z_{m2} = jZ_{m0}\tan(k_m l_m/2), \quad Z_{h1} = Z_{h2} = jZ_{h0}\tan(k_h l_h/2),\\
&Z_{b3} = -jZ_{b0}/\sin(k_b l_b), \quad Z_{p3} = -jZ_{p0}/\sin(k_p l_p),\\
&Z_{m3} = -jZ_{m0}/\sin(k_m l_m), \quad Z_{h3} = -jZ_{h0}/\sin(k_h l_h),\\
&Z_{b0} = \rho_b c_b S_b, \quad Z_{p0} = \rho_p c_p S_p, \quad Z_{m0} = \rho_m c_m S_m, \quad Z_{h0} = \rho_h c_h S_h,
\end{aligned} \tag{18}$$

where k denotes longitudinal wavenumber, ρ is density, c is sound speed, and S is cross-sectional area. Z_{ml} is the mechanical load, i.e., the mechanical impedance of the radiating plate (Eq. (17)). The clamped capacitance C_0 and the electro-mechanical conversion coefficient N are given as

$$C_0 = p^2 S_p \epsilon_{33}^T(1-k_{33}^2)/l_p, \quad N = pd_{33}S_p/(s_{33}^E l_p), \tag{19}$$

where $k_{33}^2 = d_{33}^2/(\epsilon_{33}^T s_{33}^E)$ is the electromechanical coupling coefficient, and p is the number of piezoceramic discs. Finally, we can set the matrix equation by applying Kirchhoff's circuit laws, so the velocity responses of each part ($u_1, \ldots, u_5$, see Figs. 1 and 3) of the transducer can be

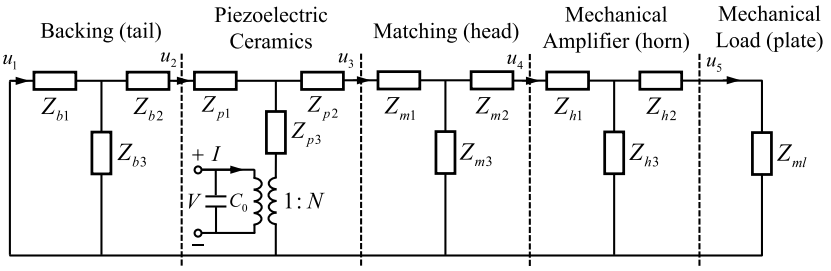

Fig. 3. Equivalent circuit model of the flat plate transducer.

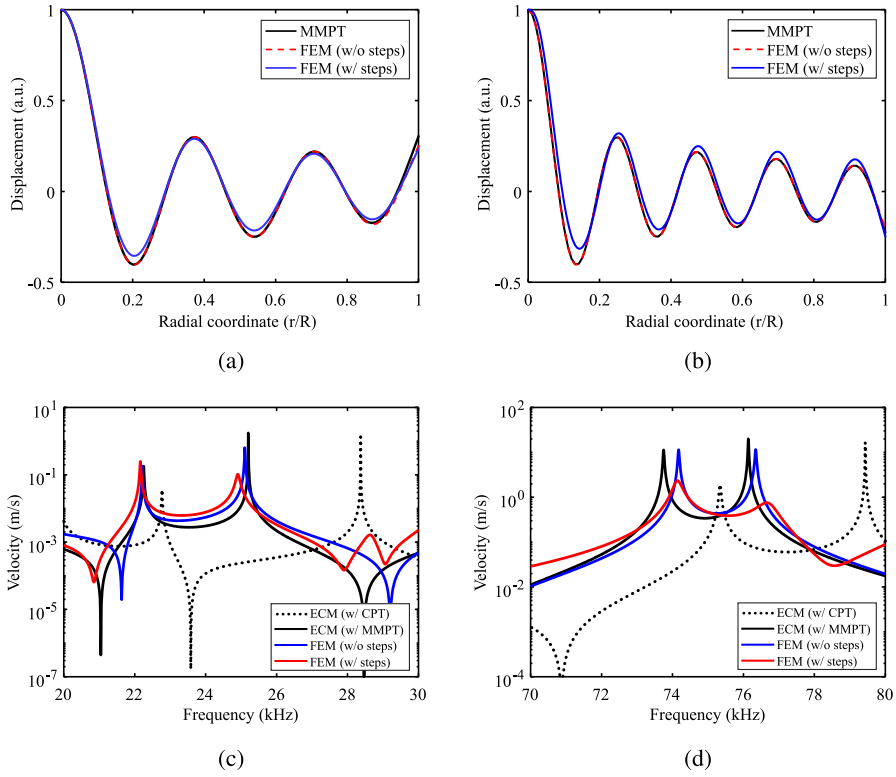

Fig. 4. Dynamic characteristics of the transducers: (a)–(b) Mode shapes of the plates. (c)–(d) Velocity responses: ECM with mechanical impedance of the plate from the CPT (dotted), ECM with mechanical impedance of the plate from the MMPT (black solid), FEM without (blue lines) and with steps (red lines).

obtained from the following relation

$$\begin{bmatrix} Z_{11} & Z_{12} & 0 & 0 & 0 \\ Z_{21} & Z_{22} & Z_{23} & 0 & 0 \\ 0 & Z_{32} & Z_{33} & Z_{34} & 0 \\ 0 & 0 & Z_{43} & Z_{44} & Z_{45} \\ 0 & 0 & 0 & Z_{54} & Z_{55} \end{bmatrix} \begin{Bmatrix} u_1 \\ u_2 \\ u_3 \\ u_4 \\ u_5 \end{Bmatrix} = \begin{Bmatrix} 0 \\ -NV \\ NV \\ 0 \\ 0 \end{Bmatrix}, \tag{20}$$

where $Z_{11} = -(Z_{b1} + Z_{b3})$, $Z_{12} = Z_{21} = Z_{b3}$, $Z_{22} = -(Z_{b1} + Z_{b3} + Z_{p1} + Z_{p3})$, $Z_{23} = Z_{32} = Z_{p3}$, $Z_{33} = -(Z_{p1} + Z_{p3} + Z_{m1} + Z_{m3})$, $Z_{34} = Z_{43} = Z_{m3}$, $Z_{44} = -(Z_{m1} + Z_{m3} + Z_{h1} + Z_{h3})$, $Z_{45} = Z_{54} = Z_{h3}$, and $Z_{55} = -(Z_{h1} + Z_{h3} + Z_{ml})$.

4. Numerical design examples

In this section, we present numerical design examples for two transducers (Table A.2) that have different target frequencies, and therefore can be used for different purposes. Among the various applications of SPTs, we chose a source transducer for harmonic radiation force generation [8] with a operating frequency of 25 kHz and a PA source [10,11] with a target frequency of 75 kHz as design examples.

As a first example, we design the transducer with a 25 kHz operating frequency. We adopt a previous design of a SPT for source transducer of harmonic force generation [8]. For detailed design of the plate's complex geometrical shape, the authors used Genetic algorithm [49] and the modal assurance criterion to match the mode shape and resonant frequencies. Here, we will demonstrate that the SPT can be designed without complicated design process by exploiting the advantages of polymer-composite steps. We selected a plate with a radius of 150 mm and a thickness of 7.3 mm, similar to the dimensions designed in [8]. We used a polymer-composite that has a density of 500 kg/m^3, Young's modulus of 1.5 GPa, and Poisson's ratio of 0.23. The plate had h/R = 0.049, with eigenmode and frequency calculated using MMPT are 6 th and 25.04 kHz, respectively. The position and height of the steps can be easily determined by the nodal points of the mode shape and the half-wavelength that corresponds to the eigenfrequency [11]. Detailed geometries and dimensions of the steps are described in Fig. A.1, Table A.3. As shown in Fig. 4(a), comparison of the mode shapes calculated by MMPT (without steps), and FEM (without steps and with steps) show that the presence of steps does not significantly affect the mode shape. The Langevin transducer is a half-wavelength resonator [16], so this part can be designed to have near the target frequency. In Fig. 4(c), the resonant frequencies near the target frequency (25 kHz) were 25.2 kHz (calculated using ECM with the mechanical impedance

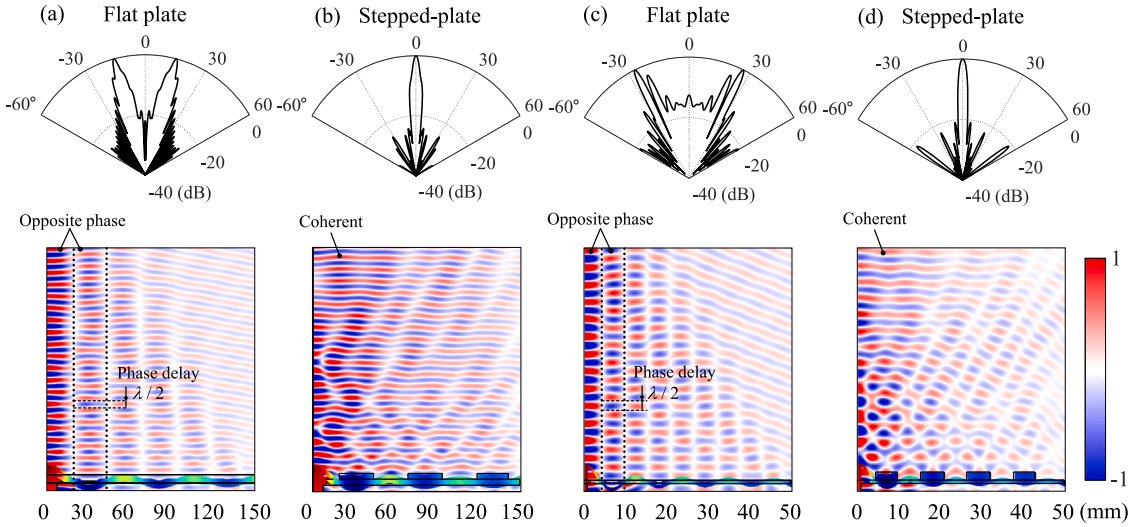

Fig. 5. Acoustic pressure field and far-field beam patterns of the flat plate transducers and stepped-plate transducers of first ((a)–(b)) and second ((c)–(d)) design examples, respectively.

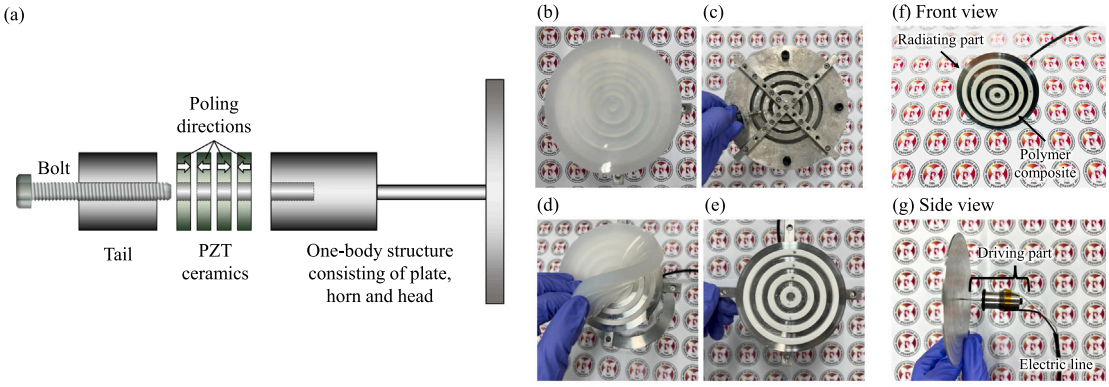

Fig. 6. (a) Cross-sectional schematic of the transducer components. Fabrication process of the polymer composite steps: (b) mounted silicone mold on the jig for polymer injection, (c) injection of liquid polymer composite, (d) detaching the silicone mold after curing, and (e) gate mark removal and surface polishing. Photographs of the fabricated transducer: (f) front and (g) side views.

of the plate obtained by MMPT), 25.1 kHz (without steps, calculated using FEM), and 24.9 kHz (with steps, calculated using FEM). The response of the ECM with MMPT is substantially comparable to that of FEM without steps, whereas ECM with CPT deviate from it. Attaching the polymer steps caused only a negligible shift in resonance frequency. The velocity response curve without steps had a similar tendency to the others that include the steps; this comparison implies that the intricate design procedure for the conventional SPT can be simplified by using polymer-composite steps.

As a second example, we designed the PCSPT with the purpose of using it as a source for PAs [11] that have a target frequency of around 75 kHz. We selected a radiating plate that had a diameter of 50 mm and a thickness of 1 mm. In this case, $h/R = 0.02$ and the mode number and frequency calculated using MMPT are 9 th and 74.94 kHz. The driving component is built in a similar fashion to the first example. In Fig. 4(d), the resonant frequencies near the target frequency were 76.1 kHz (calculated using ECM with MMPT), 76.3 kHz (without steps, calculated using FEM), and 76.3 kHz (with steps, calculated using FEM). The difference in mode shape (illustrated in Fig. 4(b)) and in resonant frequency are insignificant after the steps are implemented; these results are similar to the previous example. The material properties of polymer composites can be tailored to minimize their influence on the resonant frequencies and mode shapes. We will explore this idea in subsequent work.

The far-field beam patterns and acoustic pressure field (Fig. 5) of the designed transducers demonstrate the effects of the polymer steps. The plate transducers that lack steps suffer from poor directivity due to destructive interference caused by the incoherent phase of bending modes. In contrast, the stepped-plate transducers form coherent as a result of the half-wavelength spatial delay imposed by the steps; and consequently, generate highly-directional waves. In summary, the light and flexible nature of the polymer composite steps has little effect on the mechanical behavior of the radiating plate; therefore, use of these steps enables adequate design without considering the steps in the theoretical model. In addition, the developed ECM loosens constraints on geometry and target frequency, and thereby enables development of high-power ultrasonic transducers for a wide range of applications. A reliable wide-band frequency response of transducers that have thin to moderately-thick plates can be achieved.

5. Experimental results

5.1. Transducer fabrication

In this study, the PA source transducer i.e., the second designed transducer, was fabricated Fig. 6(a) for experimental testing. All part except the PZT ceramics were manufactured by machining. All the components are fastened with a bolt to complete the assembly. A

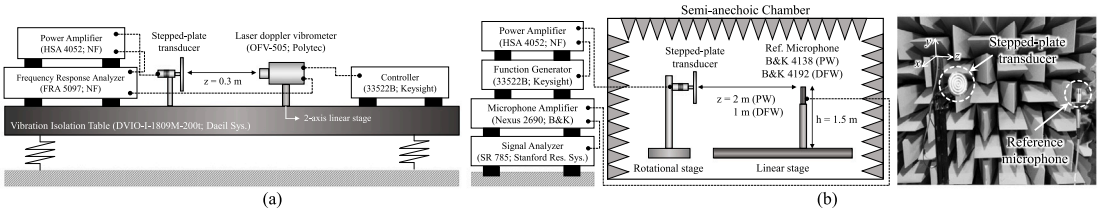

Fig. 7. Experimental setup for (a) vibration and (b) acoustic characteristics measurements.

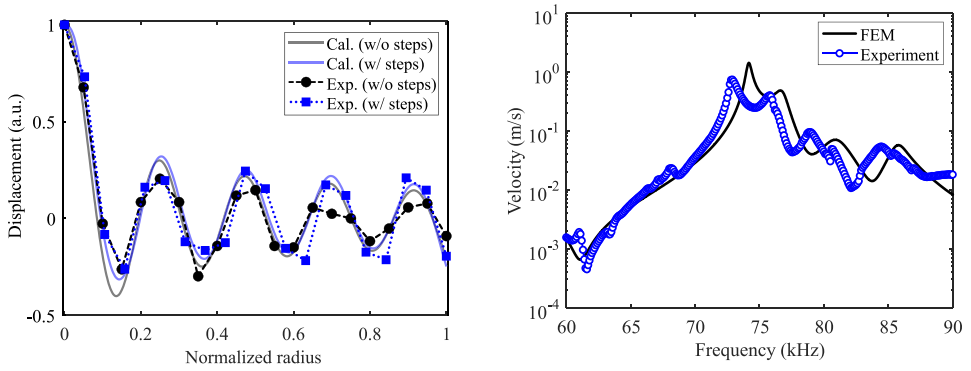

Fig. 8. Vibration characteristics of the transducer: (a) Ninth mode shape and (b) velocity response. Both experimental results are compared with the predictions.

polytetrafluoroethylene (PTFE) tube was inserted between the bolt and PZT ceramics to prevent electrical breakdowns, which may occur when driving voltage is high [10,11]. The polymer-composite steps can be easily fabricated using the silicone mold as described in [11]. The fabrication process of the polymer-composite steps is shown in Fig. 6(b)–(e). Fig. 6(f) and Fig. 6(g) show the front and side views of the fabricated transducer.

5.2. Experimental set-up

The experiment involved measurement of vibration characteristics and acoustic characteristics, specifically. Fig. 7(a) shows the experimental setup for measuring the mode shapes and velocity responses. The input electric signal generated by the frequency response analyzer (FRA 5097; NF Corporation) was amplified by the power amplifier (HSA 4052; NF Corporation) and a voltage of 10 V_{pk} was applied. The vibration characteristics of the transducer were measured using a laser Doppler vibrometer (OFV-505; Polytec) and a controller (OFV-5000; Polytec). The measured signal was visualized by the frequency response analyzer. The mode shape was measured by using a linear stage to move the transducer in the radial direction. The acoustic measurements (Fig. 7(b)) were conducted in a semi-anechoic chamber (3 m × 3 m × 2 m). The input signal was applied to the transducer by using a function generator (33522B; Keysight) and a power amplifier (HSA 4052; NF Corporation). The primary waves were measured using a high-frequency calibrated reference microphone (1/8″ Type 4138; Brüel & Kjær), and the difference frequency waves were measured using an audio-frequency calibrated reference microphone (1/2″ Type 4192; Brüel & Kjær). The measured acoustic signal was amplified using a microphone amplifier (Nexus 2690; Brüel & Kjær) then analyzed using a signal analyzer (SR 785; Stanford Research Systems).

5.3. Vibration measurements

The mode shapes were obtained by measuring the velocities at multiple points on the flat and the stepped plates. The frequency response was estimated relative the center velocity of the plate. The

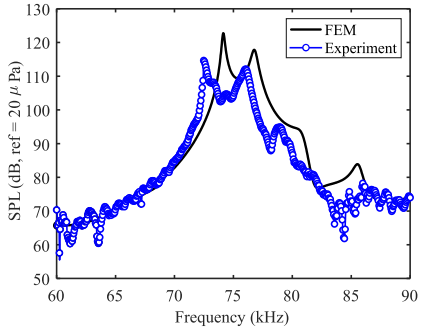

Fig. 9. Predicted and measured sound pressure levels of the primary waves.

measurement range was 60 kHz to 90 kHz, which covers the operating frequency. Fig. 8(a) shows a comparison of the predicted and experimental results for the ninth-order mode shape before and after the steps were attached. We can see that the plate behaved in the desired flexural mode even after the steps are attached. The calculated and measured velocity responses (Fig. 8(b)) show some errors, which probably occurred because of structural asymmetry and slight differences in boundary conditions and mechanical properties. Nevertheless, the measurement results tended to agree with the calculated results.

5.4. Acoustic measurements

5.4.1. Primary waves

Primary waves are high-frequency ultrasounds that are emitted directly from the transducer. To accurately detect the primary waves, a microphone with a flat sensitivity up to the high-frequency range is required; therefore, we used a high-frequency 1/8″ microphone. To avoid near-field interference, the 1/8″ microphone was placed 2 m from the Rayleigh range ($\pi r_{plate}^2/\lambda_{PW} = 1.72$ m) that represents the far-field region.

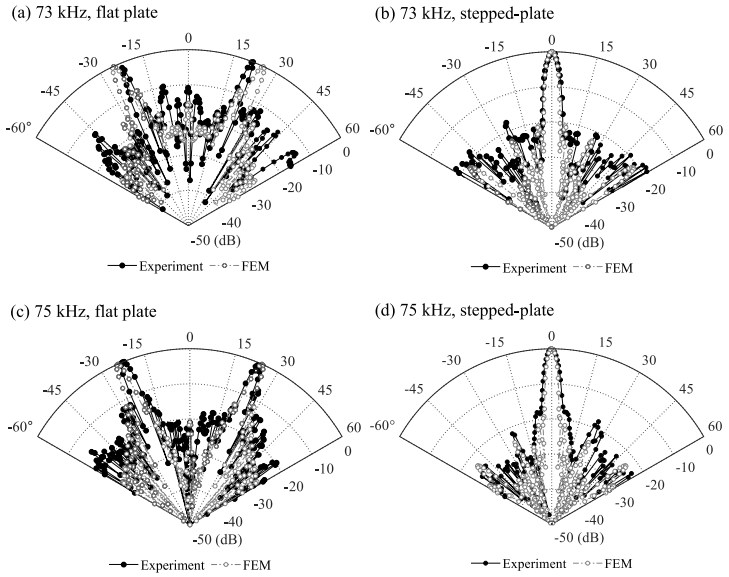

Fig. 10. Beam patterns of the transducer with and without steps around the target ultrasonic frequency.

The measured sound pressure level (SPL) of the primary waves show two resonant peaks, one at 72.8 kHz and one at 76.1 kHz for SPL of 115 dB and 112 dB, respectively, which agree well with the FEM results at 74.1 kHz and 76.6 kHz; the relative error for the resonant frequencies is 1.5% and 0.9%, respectively (Fig. 9). One important characteristic of the PCSPT is the sound directivity, which is clear from the beam patterns. Measured and predicted beam patterns (Fig. 10) were obtained in the range from −60° to 60°. The flat plate cannot generate directional waves because of the strong destructive interference whereas highly-directional waves are formed after the polymer-composite steps are attached. The experimental results were in good agreement with the predictions, and the half-power beamwidth (HPBW) of all the beam patterns were ≤5°; the sidelobe levels were ≥15 dB.

5.4.2. *Difference frequency waves*

The fabricated transducer in this work can be used as a PA directional loudspeaker [10,11]. The difference frequency wave (DFW), which is a PA sound, has a frequency that is the difference between the two primary frequencies. To produce a DFW sound, a modulated input signal is required. The input electrical signal to generate the PA sound waves is

$$V_{\text{Input}} = V_1 \sin(\omega_c t) + V_2 \sin\left[(\omega_c + \omega_m)t\right], \quad \omega_c = 2\pi f_c, \quad \omega_m = 2\pi f_m, \tag{21}$$

where f_c is the carrier frequency, and f_m is the modulation frequency that covers the audible sound range. Here, f_c was fixed at 72.8 kHz, which is the first peak that shows the highest SPL among the two resonances, and both the input voltage V_1 and V_2 were set to 25 V_{pk}. The microphone for detecting the DFW signal was positioned at a distance of 1 m from the transducer to avoid any spurious sounds. Theoretically, the SPL of a PA sound at the source is zero [50]. As the primary waves propagate, SPL of the PA increases cumulatively. However, it is often detected to be higher than the theoretical value because of the non-linearity of the receiving microphone [51]. To accurately measure the DFW sound, it must be free from any non-linear distortion signals (spurious sounds) produced by a microphone that is exposed to high-intensity primary waves [50,52]. In this study, we used an audio-frequency $1/2''$ microphone at a distance ≥1 m from the transducer to ensure that it would be free from spurious sounds because the total harmonic distortion (THD) was ≤0.01% [11]. SPL of the DFW

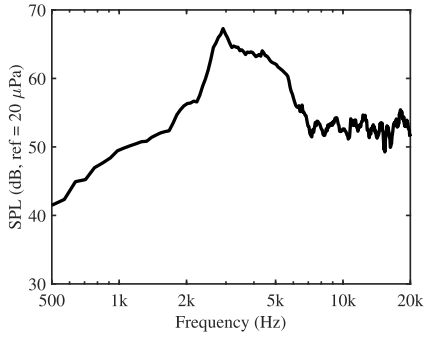

Fig. 11. Sound pressure level of the parametric array sounds (difference frequency waves).

was measured from 500 Hz to 20 kHz (Fig. 11). In Fig. 12, the measured beam patterns of DFW were compared with the results of the numerical calculations using the Khokhlov–Zabolotskaya–Kuznetsov (KZK) time-domain simulation package, called Texas code [53]. All the DFW beam patterns had HPBWs ≤5° and sidelobe levels ≥15 dB. Also, all the major lobes showed high directivity and similar narrow beam shapes for the KZK numerical results. All of these experimental results confirm that the transducer was well manufactured and that its responses are similar to those predicted.

6. Conclusions

This article has presented an analytical model to design a polymer-composite stepped-plate ultrasonic transducer. We utilized the modified Mindlin plate theory, which enables accurate calculation of the mechanical impedance of a plate, irrespective of frequency and thickness-to-radius ratio. Also, since the polymer-composite steps can be adopted for other high-power ultrasonic applications of SPT, our proposed model can enhance the design efficiency since it enormously reduces the sophisticated analysis of the vibratory response of the stepped-plate. Numerical design examples and experimental results confirmed that

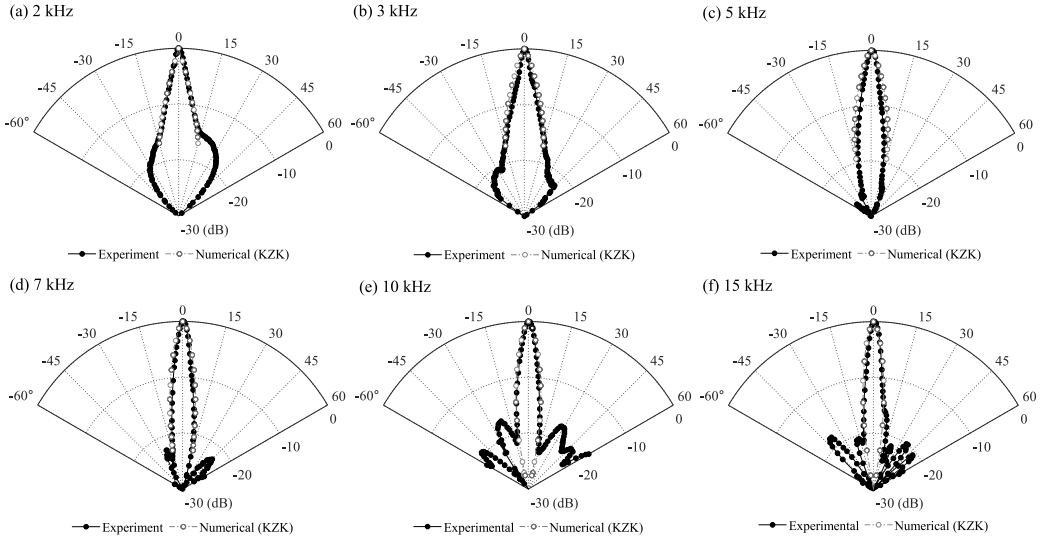

Fig. 12. Beam patterns of the difference frequency waves: (a) f_m = 2 kHz, (b) 3 kHz, (c) 5 kHz, (d) 7 kHz, (e) 10 kHz, and (f) 15 kHz.

effective design procedure can be achievable without considering the steps in the theoretical model, so the process of designing a stepped-plate transducer is now simplified. Our findings suggest that PCSPTs can be simply designed by using the analytic model presented in this work and used in a wide range of ultrasonic applications.

CRediT authorship contribution statement

Beomseok Oh: Conceptualization, Investigation, Methodology, Software, Validation, Writing – original draft. **Chayeong Kim:** Software, Methodology. **Dongwoo Lee:** Methodology, Writing – review & editing. **Junsuk Rho:** Funding acquisition, Writing – review & editing. **Wonkyu Moon:** Conceptualization, Funding acquisition, Supervision, Writing – review & editing.

Declaration of competing interest

The authors declare that they have no known competing financial interests or personal relationships that could have appeared to influence the work reported in this paper.

Data availability

Data will be made available on request.

Acknowledgments

This work was financially supported by the National Research Foundation (NRF) grants (NRF-2019R1A2C3003129, CAMM-2019M3A6B3030637, NRF-2021M3C1C3097512) funded by the Ministry of Science and ICT (MSIT) of the Korean government, and the grant (PES4400) from the endowment project of "Development of smart sensor technology for underwater environment monitoring" funded by Korea Research Institute of Ships & Ocean engineering (KRISO).

Appendix A. Material properties and geometrical dimensions of the designed transducers

Here we provide the material properties and geometrical dimensions for the transducer designs. In the first design, we used aluminum for the transducer structure except for the piezoelectric part. And for the second, we chose steel for the tail and aluminum for the remaining components, excluding the piezoelectric ceramics.

Table A.1
Material properties.

Material	Property		Value
Aluminum (Al-7075)	Young's modulus,	E	72 GPa
	Mass density,	ρ	2780 kg/m^3
	Poisson's ratio,	ν	0.33
Steel (STS-304)	Young's modulus,	E	193 GPa
	Mass density,	ρ	7930 kg/m^3
	Poisson's ratio,	ν	0.29
PZT (C-21)	Elastic compliance,	s_{11}^E	12.0×10^{-12} m^2/N
		s_{12}^E	-3.5×10^{-12} m^2/N
		s_{13}^E	-4.5×10^{-12} m^2/N
		s_{33}^E	15.6×10^{-12} m^2/N
		s_{44}^E	43.5×10^{-12} m^2/N
	Piezoelectric	d_{31}	-131×10^{-12} m/V
	charge constants,	d_{33}	288×10^{-12} m/V
		d_{15}	634×10^{-12} m/V
	Piezoelectric	g_{31}	-10.7×10^{-3} V m/N
	voltage constants,	g_{33}	27.2×10^{-3} V m/N
		g_{15}	37.7×10^{-3} V m/N
	Dielectric constants	ε_{11}^T	1900
	(relative),	ε_{33}^T	1400
	Mass density,	ρ	7800 kg/m^3
	Poisson's ratio,	ν	0.29
	Quality factor,	Q_m	1400
	Loss factor,	$\tan\delta$	0.30%

Table A.2
Geometrical dimensions of the designed transducers (unit: mm).

	a_p	t_p	a_h	l_h	l_m	l_p	l_b	a_d
Design 1	300	7.3	9	51	51	16	40	38.2
Design 2	100	1	1.5	15.3	13.9	4	12	14

Table A.3
Detailed dimensions of the polymer-composite steps (unit: mm).

	r_{s1}	r_{s2}	r_{s3}	r_{s4}	r_{s5}	r_{s6}	r_{s7}	r_{s8}	r_{s9}
Design 1	19.5	43.5	69.5	93.3	119.1	141.2	–	–	–
Design 2	4.2	9.8	15.3	20.9	26.4	32.0	37.5	43.2	48.1

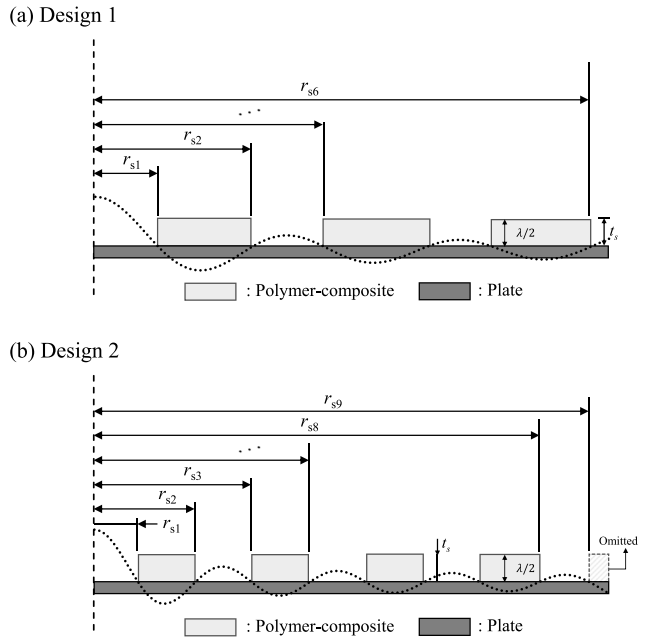

Fig. A.1. Geometries of the steps for (a) Design 1 and (b) Design 2.

Appendix B. Supplementary data

Supplementary material related to this article can be found online at https://doi.org/10.1016/j.ultras.2023.106933.

References

[1] A. Barone, J.A. Gallego Juarez, Flexural vibrating free-edge plates with stepped thicknesses for generating high directional ultrasonic radiation, J. Acoust. Soc. Am. 51 (3B) (1972) 953–959, http://dx.doi.org/10.1121/1.1912944.

[2] E. Riera, A. Cardoni, J. Gallego-Juárez, V. Acosta, A. Blanco, G. Rodríguez, M. Blasco, L. Herranz, Recent advances in the development and application of power plate transducers in dense gas extraction and aerosol agglomeration processes, Physics Procedia 63 (2015) 67–72, http://dx.doi.org/10.1016/j.phpro.2015.03.011, 43rd Annual UIA Symposium 23—25 April 2014 CSIC Madrid, Spain, URL https://www.sciencedirect.com/science/article/pii/S1875389215000826.

[3] T. Otsuka, K. Higuchi, K. Seya, Ultrasonic levitation by stepped circular vibrating plate, Japan. J. Appl. Phys. 29 (S1) (1990) 170, http://dx.doi.org/10.7567/jjaps.29s1.170.

[4] J. Gallego-Juárez, G. Rodriguez, J. San Emeterio, P. Sanz, J. Lázaro, An acoustic transducer system for long-distance ranging applications in air, Sensors Actuators A 37–38 (1993) 397–402, http://dx.doi.org/10.1016/0924-4247(93)80068-R, Proceedings of Eurosensors VI, URL https://www.sciencedirect.com/science/article/pii/092442479380068R.

[5] J. Park, Y. Je, H. Lee, W. Moon, Design of an ultrasonic sensor for measuring distance and detecting obstacles, Ultrasonics 50 (3) (2010) 340–346, http://dx.doi.org/10.1016/j.ultras.2009.10.013, URL https://www.sciencedirect.com/science/article/pii/S0041624X09001504.

[6] E. Riera, J.A. Gallego-Juárez, T.J. Mason, Airborne ultrasound for the precipitation of smokes and powders and the destruction of foams, Ultrason. Sonochemistry 13 (2) (2006) 107–116, http://dx.doi.org/10.1016/j.ultsonch.2005.04.001, URL https://www.sciencedirect.com/science/article/pii/S1350417705000337.

[7] J.A. Gallego-Juárez, E. Riera, S. de la Fuente Blanco, G. Rodríguez-Corral, V.M. Acosta-Aparicio, A. Blanco, Application of high-power ultrasound for dehydration of vegetables: Processes and devices, Drying Technol. 25 (11) (2007) 1893–1901, http://dx.doi.org/10.1080/07373930701677371.

[8] G.V. Selicani, F. Buiochi, Stepped-plate ultrasonic transducer used as a source of harmonic radiation force optimized by genetic algorithm, Ultrasonics 116 (2021) 106505, http://dx.doi.org/10.1016/j.ultras.2021.106505, URL https://www.sciencedirect.com/science/article/pii/S0041624X21001359.

[9] Y. Je, H. Lee, J. Park, W. Moon, A stepped-plate bi-frequency source for generating a difference frequency sound with a parametric array, J. Acoust. Soc. Am. 127 (6) (2010) 3494–3502, http://dx.doi.org/10.1121/1.3397445.

[10] Y. Hwang, W. Moon, A wide-band in-air parametric array source composed of a circular plate with steps and a Langevin transducer with a horn, Appl. Acoust. 141 (2018) 223–233, http://dx.doi.org/10.1016/j.apacoust.2018.07.022, URL https://www.sciencedirect.com/science/article/pii/S0003682X16304133.

[11] C. Kim, Y. Hwang, K. Shin, W. Moon, A parametric array loudspeaker featuring a langevin transducer, a circular aluminum plate, and composite polymer steps, Sensors Actuators A 338 (2022) 113466, http://dx.doi.org/10.1016/j.sna.2022.113466, URL https://www.sciencedirect.com/science/article/pii/S0924424722001042.

[12] G. Li, J. Qu, L. Xu, X. Zhang, X. Gao, Study on multi-frequency characteristics of a longitudinal ultrasonic transducer with stepped horn, Ultrasonics 121 (2022) 106683, http://dx.doi.org/10.1016/j.ultras.2022.106683, URL https://www.sciencedirect.com/science/article/pii/S0041624X22000014.

[13] P.J. Westervelt, Parametric acoustic array, J. Acoust. Soc. Am. 35 (4) (1963) 535–537, http://dx.doi.org/10.1121/1.1918525.

[14] Y. Hwang, W. Moon, Y. Je, W. Kim, S. Lee, A precise equivalent-circuit model for a circular plate radiator, Acta Acust. United Acust. 104 (1) (2018) 79–86.

[15] I. Senjanović, N. Vladimir, M. Tomić, An advanced theory of moderately thick plate vibrations, J. Sound Vib. 332 (7) (2013) 1868–1880, http://dx.doi.org/10.1016/j.jsv.2012.11.022, URL https://www.sciencedirect.com/science/article/pii/S0022460X12009169.

[16] C.H. Sherman, J.L. Butler, Transducers and Arrays for Underwater Sound, Vol. 4, Springer, 2007.

[17] S. Hirose, M. Aoyagi, Y. Tomikawa, Dielectric loss in a piezoelectric ceramic transducer under high-power operation; increase of dielectric loss and its influence on transducer efficiency, Japan. J. Appl. Phys. 32 (Part 1, No. 5B) (1993) 2418–2421, http://dx.doi.org/10.1143/jjap.32.2418.

[18] S. Hirose, New method for measuring mechanical vibration loss and dielectric loss of piezoelectric transducer under high-power excitation, Japan. J. Appl. Phys. 33 (Part 1, No. 5B) (1994) 2945–2948, http://dx.doi.org/10.1143/jjap.33.2945.

[19] S. Takahashi, M. Yamamoto, Y. Sasaki, Nonlinear piezoelectric effect in ferroelectric ceramics, Japan. J. Appl. Phys. 37 (Part 1, No. 9B) (1998) 5292–5296, http://dx.doi.org/10.1143/jjap.37.5292.

[20] T. Li, Y. Chen, J. Ma, Frequency dependence of piezoelectric vibration velocity, Sensors Actuators A 138 (2) (2007) 404–410, http://dx.doi.org/10.1016/j.sna.2007.05.024, URL https://www.sciencedirect.com/science/article/pii/S0924424707004372.

[21] M. Umeda, K. Nakamura, S. Ueha, Effects of vibration stress and temperature on the characteristics of piezoelectric ceramics under high vibration amplitude levels measured by electrical transient responses, Japan. J. Appl. Phys. 38 (Part 1, No. 9B) (1999) 5581–5585, http://dx.doi.org/10.1143/jjap.38.5581.

[22] R. Andrés, V. Acosta, M. Lucas, E. Riera, Modal analysis and nonlinear characterization of an airborne power ultrasonic transducer with rectangular plate radiator, Ultrasonics 82 (2018) 345–356, http://dx.doi.org/10.1016/j.ultras.2017.09.017, URL https://www.sciencedirect.com/science/article/pii/S0041624X17304146.

[23] J. Gallego-Juarez, G. Rodriguez-Corral, L. Gaete-Garreton, An ultrasonic transducer for high power applications in gases, Ultrasonics 16 (6) (1978) 267–271, http://dx.doi.org/10.1016/0041-624X(78)90053-7, URL https://www.sciencedirect.com/science/article/pii/0041624X78900537.

[24] O.E. Mattiat, Ultrasonic Transducer Materials, Springer Science & Business Media, 2013.

[25] A. Abdullah, M. Shahini, A. Pak, An approach to design a high power piezoelectric ultrasonic transducer, J. Electroceram. 22 (4) (2009) 369–382.

[26] A.W. Leissa, Vibration of Plates, Vol. 160, Scientific and Technical Information Division, National Aeronautics, 1969.

[27] E. Reissner, The effect of transverse shear deformation on the bending of elastic plates, J. Appl. Mech. 12 (2) (1945) A69–A77.

[28] R.D. Mindlin, Influence of rotatory inertia and shear on flexural motions of isotropic, elastic plates, J. Appl. Mech. 18 (1) (1951) 31–38.

[29] E. Reissner, On the theory of transverse bending of elastic plates, Int. J. Solids Struct. 12 (8) (1976) 545–554, http://dx.doi.org/10.1016/0020-7683(76)90001-9, URL https://www.sciencedirect.com/science/article/pii/0020768376900019.

[30] R. Szilard, Elastic plate theories and their governing differential equations, in: Theories and Applications of Plate Analysis, John Wiley & Sons, Ltd, 21–61, http://dx.doi.org/10.1002/9780470172872.ch1, URL https://onlinelibrary.wiley.com/doi/abs/10.1002/9780470172872.ch1.

[31] U. Gupta, R. Lal, S. Sharma, Vibration of non-homogeneous circular Mindlin plates with variable thickness, J. Sound Vib. 302 (1) (2007) 1–17, http://dx.doi.org/10.1016/j.jsv.2006.07.005, URL https://www.sciencedirect.com/science/article/pii/S0022460X06005670.

[32] J.A. Gallego-Juarez, Piezoelectric ceramics and ultrasonic transducers, J. Phys. E: Sci. Instrum. 22 (10) (1989) 804–816, http://dx.doi.org/10.1088/0022-3735/22/10/001.

[33] C. Wang, Y. Xiang, E. Watanabe, T. Utsunomiya, Mode shapes and stress-resultants of circular Mindlin plates with free edges, J. Sound Vib. 276 (3) (2004) 511–525, http://dx.doi.org/10.1016/j.jsv.2003.08.010, URL https://www.sciencedirect.com/science/article/pii/S0022460X03009416.

[34] K. Liew, Y. Xiang, S. Kitipornchai, Research on thick plate vibration: a literature survey, J. Sound Vib. 180 (1) (1995) 163–176, http://dx.doi.org/10.1006/jsvi.1995.0072, URL https://www.sciencedirect.com/science/article/pii/S0022460X85700727.

[35] I. Senjanović, N. Vladimir, N. Hadžić, Modified Mindlin plate theory and shear locking-free finite element formulation, Mech. Res. Commun. 55 (2014) 95–104, http://dx.doi.org/10.1016/j.mechrescom.2013.10.007, URL https://www.sciencedirect.com/science/article/pii/S009364131300164X.

[36] I. Senjanovic, N. Hadzic, N. Vladimir, D.-S. Cho, Natural vibrations of thick circular plate based on the modified Mindlin theory, Arch. Mech. 66 (6) (2014) 389–409.

[37] N. Stephen, Mindlin plate theory: best shear coefficient and higher spectra validity, J. Sound Vib. 202 (4) (1997) 539–553, http://dx.doi.org/10.1006/jsvi.1996.0885, URL https://www.sciencedirect.com/science/article/pii/S0022460X96908858.

[38] K. Itao, S.H. Crandall, Natural modes and natural frequencies of uniform, circular, free-edge plates, J. Appl. Mech. 46 (2) (1979) 448–453, http://dx.doi.org/10.1115/1.3424569.

[39] R.H. Lyon, Drive-point functions and modal density, J. Acoust. Soc. Am. 121 (2) (2007) EL62–EL63, http://dx.doi.org/10.1121/1.2424266.

[40] D.S. Cho, B.H. Kim, J.-H. Kim, N. Vladimir, T.M. Choi, Forced vibration analysis of arbitrarily constrained rectangular plates and stiffened panels using the assumed mode method, Thin-Walled Struct. 90 (2015) 182–190, http://dx.doi.org/10.1016/j.tws.2015.01.020, URL https://www.sciencedirect.com/science/article/pii/S0263823115000300.

[41] D. Seung Cho, B. Hee Kim, J.-H. Kim, N. Vladimir, T. Muk Choi, Frequency response of rectangular plate structures in contact with fluid subjected to harmonic point excitation force, Thin-Walled Struct. 95 (2015) 276–286, http://dx.doi.org/10.1016/j.tws.2015.07.013, URL https://www.sciencedirect.com/science/article/pii/S0263823115300392.

[42] W. Xiao, L. Li, S. Lei, Accurate modal superposition method for harmonic frequency response sensitivity of non-classically damped systems with lower-higher-modal truncation, Mech. Syst. Signal Process. 85 (2017) 204–217, http://dx.doi.org/10.1016/j.ymssp.2016.08.017, URL https://www.sciencedirect.com/science/article/pii/S0888327016302990.

[43] B. Fu, T. Hemsel, J. Wallaschek, Piezoelectric transducer design via multiobjective optimization, Ultrasonics 44 (2006) e747–e752, http://dx.doi.org/10.1016/j.ultras.2006.05.087, Proceedings of Ultrasonics International (UI'05) and World Congress on Ultrasonics (WCU), URL https://www.sciencedirect.com/science/article/pii/S0041624X06001223.

[44] S. Lin, L. Xu, H. Wenxu, A new type of high power composite ultrasonic transducer, J. Sound Vib. 330 (7) (2011) 1419–1431, http://dx.doi.org/10.1016/j.jsv.2010.10.009, URL https://www.sciencedirect.com/science/article/pii/S0022460X1000670X.

[45] J. Lin, S. Lin, J. Xu, Analysis and experimental validation of longitudinally composite ultrasonic transducers, J. Acoust. Soc. Am. 145 (1) (2019) 263–271, http://dx.doi.org/10.1121/1.5087554.

[46] Y. Gan, B. Meng, Y. Chen, F. Sun, An intelligent measurement method of the resonant frequency of ultrasonic scalpel transducers based on PSO-BP neural network, Measurement 190 (2022) 110680, http://dx.doi.org/10.1016/j.measurement.2021.110680, URL https://www.sciencedirect.com/science/article/pii/S0263224121015426.

[47] H. Al-Budairi, M. Lucas, P. Harkness, A design approach for longitudinal–torsional ultrasonic transducers, Sensors Actuators A 198 (2013) 99–106, http://dx.doi.org/10.1016/j.sna.2013.04.024, URL https://www.sciencedirect.com/science/article/pii/S092442471300188X.

[48] L. Shuyu, Equivalent circuits and directivity patterns of air-coupled ultrasonic transducers, J. Acoust. Soc. Am. 109 (3) (2001) 949–957, http://dx.doi.org/10.1121/1.1342004, URL https://asa.scitation.org/doi/abs/10.1121/1.1342004.

[49] S. Katoch, S.S. Chauhan, V. Kumar, A review on genetic algorithm: past, present, and future, Multimedia Tools Appl. 80 (5) (2021) 8091–8126.

[50] H. Nomura, H. Sato, Influence of microphone characteristics on demodulated sound measurement in near field of parametric loudspeaker, Japan. J. Appl. Phys. 61 (SG) (2022) SG1008, http://dx.doi.org/10.35848/1347-4065/ac4078.

[51] P.J. Westervelt, Scattering of sound by sound, J. Acoust. Soc. Am. 29 (2) (1957) 199–203, http://dx.doi.org/10.1121/1.1908830.

[52] K. Ishikawa, Y. Shiraki, T. Moriya, Spurious-sound-free measurement of parametric acoustic array using optical interferometry, JASA Express Lett. 1 (11) (2021) 112801, http://dx.doi.org/10.1121/10.0007257.

[53] Y.-S. Lee, M.F. Hamilton, Time-domain modeling of pulsed finite-amplitude sound beams, J. Acoust. Soc. Am. 97 (2) (1995) 906–917, http://dx.doi.org/10.1121/1.412135.